Journal of Magnetism and Magnetic Materials 439 (2017) 259–268

Contents lists available at ScienceDirect

Journal of Magnetism and Magnetic Materials

journal homepage: www.elsevier.com/locate/jmmm

Research articles

Faster modified protocol for first order reversal curve measurements

Emilio De Biasi

CONICET, Centro Atómico Bariloche, Av. Bustillo 9500, 8400 S. C. de Bariloche, Río Negro, Argentina

ARTICLE INFO

Article history:
Received 10 March 2017
Received in revised form 2 May 2017
Accepted 4 May 2017
Available online 11 May 2017

Keywords:
FORC
New FORC protocol
Preisach model
Stoner-Wohlfarth model

ABSTRACT

In this work we present a faster modified protocol for first order reversal curve (FORC) measurements. The main idea of this procedure is to use the information of the ascending and descending branches constructed through successive sweeps of magnetic field. The new method reduces the number of field sweeps to almost one half as compared to the traditional method. The length of each branch is reduced faster than in the usual FORC protocol. The new method implies not only a new measurement protocol but also a new recipe for the previous treatment of the data. After of these pre-processing, the FORC diagram can be obtained by the conventional methods.

In the present work we show that the new FORC procedure leads to results identical to the conventional method if the system under study follows the Stoner-Wohlfarth model with interactions that do not depend of the magnetic state (up or down) of the entities, as in the Preisach model. More specifically, if the coercive and interactions fields are not correlated, and the hysteresis loops have a square shape. Some numerical examples show the comparison between the usual FORC procedure and the propose one. We also discuss that it is possible to find some differences in the case of real systems, due to the magnetic interactions. There is no reason to prefer one FORC method over the other from the point of view of the information to be obtained. On the contrary, the use of both methods could open doors for a more accurate and deep analysis.

1. Introduction

The use of FORC diagrams for the study of magnetic systems has gained popularity in the last years[1]. Numerous works use this tool to study and describe different aspects of a given magnetic system[2–12]. The use of FORC diagrams is not limited to the study of the conventional magnetic systems. Different systems can be characterized by means of this experimental technique. For example FORC diagrams have been used on the study of the long-term thermal aging in vessel steels[13], the magnetization reversal of three-dimensional nickel anti-sphere arrays[14], etc. An important field in which the FORC diagrams become a very useful tool is the Geophysics, principally in the study of magnetic rock properties [15], but in magnetic minerals in general[16,17]. In the perspective of the academic interest, but not so far away of possible application, the reversal curves are used in the study of artificial nanostructures[8,18–20].

The widespread use of FORC diagrams in several fields of research lead to the development of better protocols. As example of this, a new protocol was introduced by Zhao[21] et al. who propose change the sweeping field step creating an irregular grid in order to gain definition in the regions of interest diminishing the consuming time.

In this paper we present a variation of the usual measurement protocol of magnetization reversal curves to generate FORC diagrams. The new protocol implies an important decrease in the experimental effort. Hereinafter we shall refer to the usual protocol as UFP (usual FORC protocol) and the new proposal as NFP (new FORC protocol).

The NFP uses the information of the magnetization descending branches, which are not taken into account in the UFP. In addition, the field data points are reduced by a factor of 2 with respect to the traditional method. Then, if the sweep velocity remains constant (both in the rise and in the decrease of the field) the experimental time is reduced to almost one half. However, the implementation of the NFP requires data pre-processing before the building of the conventional FORC diagram 1·[16]. We present the basic ideas of the pre-processing algorithm, and discuss the possible differences between NFP and UFP in real systems.

2. Usual FORC protocol

Before presenting the NFP, we review the usual FORC procedure. To obtain a set of first order reversal curves the measurement protocol starts at the lowest value of H (H_{min}), as shown in the

E-mail address: debiasi@cab.cnea.gov.ar

http://dx.doi.org/10.1016/j.jmmm.2017.05.005
0304-8853/

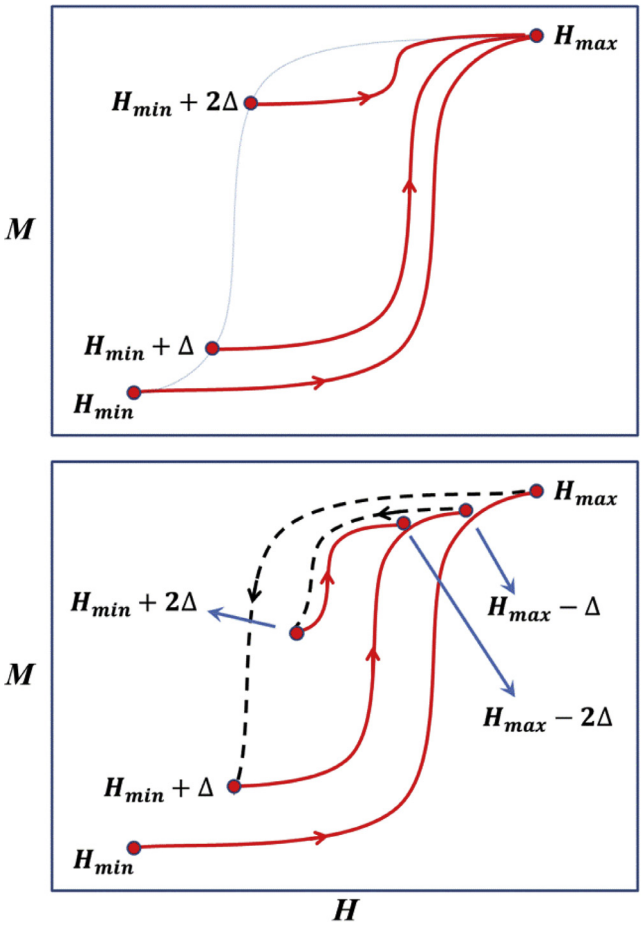

Fig. 1. Schematic representation of the measurement protocol of: (a) top panel: Usual FORC Protocol (UFP); (b) bottom panel: New FORC Protocol (NFP). The arrows indicate the sense of the field sweep. In the case of the NFP the dashed lines correspond to the descending branches.

upper panel of Fig. 1. In this figure we show the ascending branches of the UFC, labeling their initial field for more clarity. The arrows indicate the field sweep direction. The external magnetic field is swept up to the highest field H_{max} and the magnetization is measured in the process. The field is swept down to $H_0 = H_{min} + \hbar$, where Δ is the sweep field step. Again, the magnetization is recorded while the field is sweep to H_{max}. The FORC method consists in the measurement of the magnetization as a function of the external magnetic field when it is increased from different values of H_0 to H_{max}. The total magnetization of the system at the applied field H on the FORC with reversal point H_0 is denoted by $M(H_0, H)$, with $H \geqslant H_0$. A FORC distribution is defined as the mixed second derivative[22]:

$$\rho(H_0, H) = -\frac{1}{2}\frac{\partial^2 M(H_0, H)}{\partial H_0 \partial H} \quad (1)$$

and the FORC diagram is the contour plot of this distribution.

In this procedure the magnetic field must be swept successively in opposite directions. However, only the ascending branches (AB) are used in the computation for the diagram calculation.

3. The modified FORC protocol

3.1. Measurement protocol

The NFP starts as the usual by sweeping the magnetic field from H_{min} to H_{max} (see the bottom panel of Fig. 1). Usually $H_{min} = -H_{max}$, but this is not strictly necessary. Next, the field is inverted to $H_{min} + \Delta$ recording the magnetization DB (dashed line). The AB is swept to $H_{max} - \Delta$ and the magnetization is also recorded. This is different than the usual method in which each ascending branch reaches H_{max}. At this point, the magnetic field is inverted again to $H_{min} + 2\Delta$. The new ascending branch is measured up to $H_{max} - 2\Delta$. The procedure is repeated diminishing successively the magnitude of the magnetic field sweep, down to zero.

Summarizing the characteristics of both procedures, we can observe that in the UFP only the AB of the magnetization are recorded, at variance with the NFP in which the DB are also measured. Also, in the UFP the AB always reach H_{max}, and in the NFP the higher value of H diminishes progressively in the same manner as H_0 increase.

Let n be the number of fields used in the sweep from H_{min} to H_{max}. Then, the number of ascending and descending branches for the UFP and NFP is given by: $N_{BU} = 2(n-1)$ and $N_{BN} = n$, respectively. Then for $n \gg 1$ we have $N_{BU} \sim 2N_{BN}$, which means that the new method reduces the number of branches by a factor of two. In addition, the fact that the NFP uses the descending branch information helps to reduce the length of the branch compared to the usual method. In effect, if we compare the number of points used in each method we have: $N_{UPF} = (n-1)^2 + 2$ and $N_{NPF} = n(n-1)/2 + 1$, respectively. It is important to mention that the value of N_{UPF} considered here takes into account the descending branch, despite this information is not used in this method. Then the ratio $\Gamma = N_{NPF}/N_{UPF} = (1/2)[1 + 1/(n - 1 + 2/(n-1))]$ shows that the new method diminishes almost to a one half the length of the magnetic field sweep. We want to emphasize that in the case that the sweep ratio is constant in both, ascending and descending cases, the ratio Γ shows, for practical purposes ($n \gg 1$), that the experimental time spent in the NFP is almost one half the associated to the UFP.

Following the above mentioned concepts, we analyze the real number of data used in each method. The conventional method actually uses $n_{UFP} = n(n+1)/2$ points corresponding to the AB only. On other hand, the number of points used in the NFP is $n_{NPF} = N_{NPF} = 1 + n(n-1)/2$, that it to say, that all points are used in this case. If we compute the difference obtain: $n_{UPF} - n_{NPF} = n - 1$. This could suggest that the new method uses less information than the usual one. This does not really happen. The reason is that the points that act as links between AB and DB must be considered twice. Each one of these points H_i corresponds to the final part of a given branch (H_{0i}, H_i), and also to the initial ordered pair (H_i, H_i) of the following branch. Because we have $N_{BN} = n$ then, the number of links is precisely $n - 1$. On other hand, if we consider the new coordinate space[22] $(\tilde{H}_c, \tilde{H}_u)$ in which the FORC density is plotted, we can observe that for both protocols the number of points is the same, and spatially arranged in the same way. In order to illustrate these concepts, we show in Fig. 2 a schematic representation of the above mentioned ideas. In this particular example we take $n = 7$. The left panels (A) and (C) of Fig. 2 correspond to the UFP and the right ones (B) and (D) to the NFP. The top panels show an illustration of the branch corresponding to each method[23], and the bottom ones all the points associated to the $(\tilde{H}_c, \tilde{H}_u)$ space. We use the following definitions: for the ascending branches (of UFP and NFP): $\tilde{H}_C = (H - H_0)/2$, $\tilde{H}_u = -(H + H_0)/2$. For the descending branches (of NFP): $\tilde{H}_u = -(H + H_0)/2$. The minus sign in the $\tilde{H}_u$ definition is for plot in the positive region of the H_u the cases H_i positive. In both cases H_0 is the initial field of the branch.

There are some important characteristics that we can observe in Fig. 2. The first one is the way in which the AB and DB of the NFP are placed in the $(\tilde{H}_c, \tilde{H}_u)$ space. The AB are arranged at the top

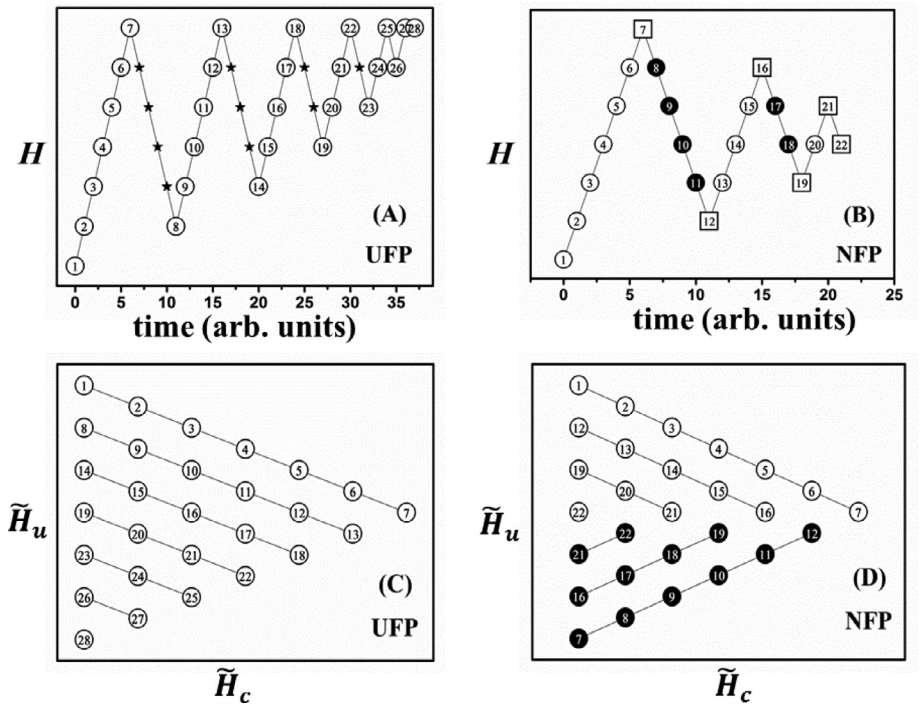

Fig. 2. Schematic representation of the UFP and NFP for the particular case $n = 7$. Uppers panels (A) and (B) represent magnetic field sweeping as function of the time (assuming a constant sweep speed). The open labeled circles correspond to the successive values of field. The black starts indicate the return of H from $Hmax$ to the beginning of the next branch. The label inside each dot indicates the order in which a given H is achieved. Panel (B) (associated to the NFP) shows three kinds of dots: open circles, corresponding to the AB; full circles, to DB; and open squares, associated to the links values of H between the AB and DB. Bottom panels (C) and (D) represent the same set of elements in the (H_c, H_u) space for the UFP and NFP respectively. The continuous lines that join the points help to visualize how the branches of the upper panels are accommodated in the lower ones.

$(\tilde{H}_u \geqslant 0)$, where the DB are placed at the bottom $(\tilde{H}_u < 0)$. The second is to observe that the linker dots appear twice in the $(\tilde{H}_c, \tilde{H}_u)$ space (once for the AB and other for the DB). Top of Fig. 2 help us to compare (for the particular case of $n = 7$) the time spend in each protocol. In the bottom panels it is possible to observe that the number of points $(\tilde{H}_c, \tilde{H}_u)$ corresponding to both methods is the same. Then, we can conclude that the $(\tilde{H}_c, \tilde{H}_u)$ space has the same number of points for both methods. This fact is a "good signal" of the proposed method, however this fact does not guarantee that the collected information is the same in both methods. By this reason, we need to ensure that the AB and DB of the NFP have the same information as at corresponding to the UFP branches. We will deal with this important issue from two points of view. First, through an example that will help us gain insight into what is happening. In second place, we will return to this topic in greater depth in Appendix I.

3.1.1. The magnetic model

With the purpose to present a numerical example we will previously expose the basic postulates of our model. We will assume that the magnetic moments behave according to the Stoner-Wohlfarth model. The interactions are included as an additional field which has a known distribution. In this sense, we can say that the interaction follows the Preisach picture[24,25]. Specifically we postulate that:

(1) The magnetization is built as the addition of square loops, which are called hysterons. This shape comes from the Stoner-Wohlfarth model.
(2) We will assume that each hysteron is an individual entity. The interaction over a given hysteron can be represented by a local internal field H_{int}, which is independent of the magnetic state (up or down) of the other hysterons.
(3) Each hysteron has a magnetization normalized to 1 and can be characterized completely by a coercive field H_c and an interaction field H_{int}. There is a function $m(H_0, H, H_c, H_{int})$ which determines completely the magnetic state (up or down) of each magnetic entity (hysteron).
(4) We will assume that the fields H_c and H_{int}, are an intrinsic property of each magnetic entity, that is, they do not depend on the magnetic state and are also independent between them.
(5) We will assume that there is a coercive fields distribution $f(H_c)$ and interaction fields distribution $g(H_{int})$. Then, the total magnetization can be expressed as:

$$M = \sum_j f(H_c^j)\{\sum_k g(H_{int}^k) m(H_0, H, H_c^j, H_{int}^k)\} \tag{2}$$

Under these hypotheses, we will show an example in order to illustrate the ideas that we have been exposed previously.

In Fig. 3 we show an example in which we have simulated the UFP and NFP. In all the numerical examples we have used $h = H/H_{max}$ (reduced external magnetic field), $h_{int} = H_{int}/H_{max}$ (reduced internal interaction field), and $h_c = H_c/H_{max}$ (reduced coercive field). For the particular case of the Fig. 3, we have used normal distributions for h_c and H_{int} fields, with mean values of $h_c \approx 0.27$ and $h_{int} = 0$, dispersions $\sigma_{h_c} \approx 0.07$ and $\sigma_{h_{int}} = 0.07$, respectively.

It is useful to first analyze the branches corresponding to both methods. In the NFP, the problem is naturally separated in two: the AB gives us the information about all the magnetic entities that have an interaction field H_{int} which satisfy the relation $H_{int} \geqslant (H_{min} + H_{max} - \Delta H)/2$ where H_{min} and H_{max} are the lowest and highest magnetic fields, respectively. On other hand, the DB contains the information for the $H_{int} < (H_{min} + H_{max} - \Delta H)/2$ cases.

Fig. 3 is divided in four panels. In panel (A) we show the branches corresponding to UFP, in panels (B) and (C), the AB and

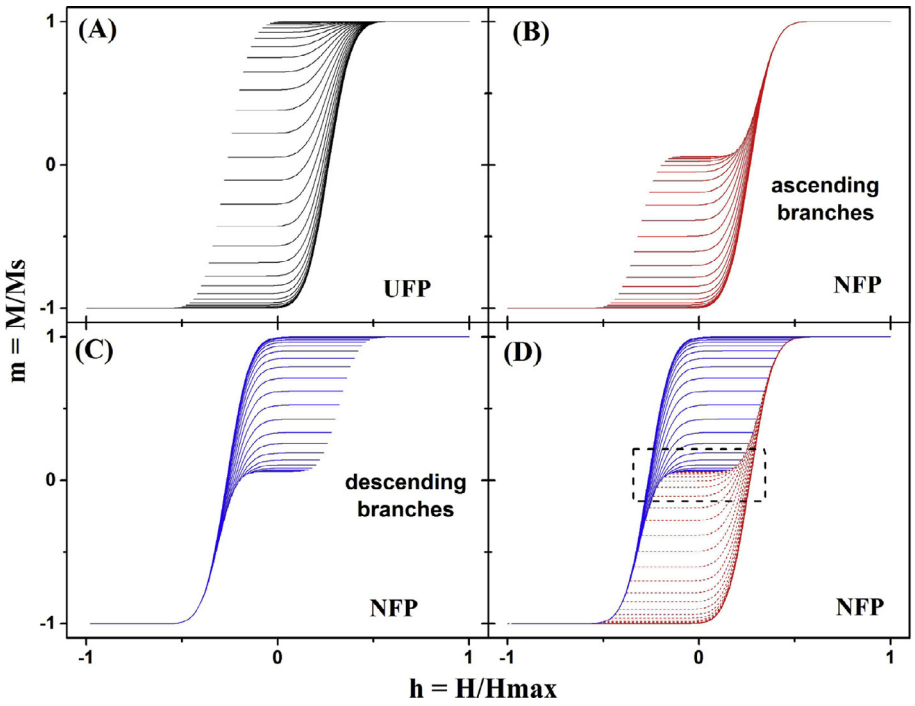

Fig. 3. Magnetic branches of a particular example (see the text) for the UFP (panel (A)) and NFP (panels (B), (C) and (D)).

DB of NFP respectively and finally in panel (D) the AB and DB together. We can see in the figure that the ascending branches of the NFP are identical to those corresponding to the UFP except in the region that divides the ascending and descending branches. The last panel shows that both branches, AB and DB, fill the space occupied by the hysteresis loop area, as the AB in the case of the UFP. This fact does not imply that both methods offer the same information, however an indication of this fact is. While the lower ascending branches coincide perfectly with those of the UFP method, the higher descending ones would correspond to a hypothetical FORC (UFP) in which the magnetic field is swept descending and starting at H_{max}. However, as we move to the frontier that divides AB and DB, the AB began to differentiate of the usual protocol. This happens because the sweep field becomes small in the interference (dashed box in Fig. 3(D)).

In order to continue with the analysis we can build the FORC diagrams corresponding to the AB and DB and put this information together in a unique plot (see Fig. 4(A)). Fig. 4(B) corresponds to the UFP treatment, for comparison. We can observe that both diagrams are identical with the exception of the region close to $h_U \approx 0$. This result is expected based on the previously exposed ideas and also the way in which the AB and DB are accommodated in the $(\tilde{H}_c, \tilde{H}_u)$ plane (see Fig. 2(D)). The big difference observed is due to the fact that, when we calculated separately with the ascending and descending branches, we did not have information about the neighborhood branches in the frontier indicated in Fig. 3 (D). We will then focus in the use all the available information to correctly calculate the FORC diagram using the AB and DB. The main idea of the processing method consists in retrieving or reproducing the AB of the UFP with the information available from the NFP.

3.1.2. Algorithm description

We will use matrices and vectors with the following convention: all matrices start from the $(0, 0)$ indexes. However, the vectors can start from a no null index value, as we will opportunely indicate. This choice helps us to simplify the description of the algorithm.

3.1.3. The UFP data treatment

In the UFP processing it is usual to store the branches information in two associated matrixes, that we will call $\boldsymbol{U}$ and $\boldsymbol{H}$, both of $n \times n$ range. The $\boldsymbol{H}$ matrix contains information of the magnetic field, the $\boldsymbol{U}$ of the magnetization. Due to the characteristics of the measurement protocol, both matrices are triangular inferior. The $\boldsymbol{H}$ matrix is built in a simple way:

$$\boldsymbol{H}[i,j] = \begin{cases} H_{min} + i\Delta & if \quad i \geqslant j \\ 0 & if \quad i < j \end{cases} \tag{3}$$

where i and j go from 0 to n – 1. Thus the first row of $\boldsymbol{H}$ has only a no null element at $\boldsymbol{H}[0,0] = H_{min}$, and also the last row have all the elements equal to $\boldsymbol{H}[n-1,j] = H_{min} + (n-1)\Delta = H_{max}$.

Then, consistently with the $\boldsymbol{H}$ definition, the rule to fill the $\boldsymbol{U}$ matrix is the following:

$$\boldsymbol{U}[i,j] = \begin{cases} M_j(H_{min} + i\Delta) & if \quad i \geqslant j \\ 0 & if \quad i < j \end{cases} \tag{4}$$

where $M_j(H_{min} + i)$ represents the magnetization of the ascending branch j at the field $H_i = H_{min} + i$. As in the case of $\boldsymbol{H}[i,j]$ definition i and j go from 0 to n - 1. In this way, the values of the magnetization associated to the i ascending branch are placed in the i column of $\boldsymbol{U}$, so that the positions of a given magnetization value match with the position of the corresponding field in the i column of the $\boldsymbol{H}$ matrix. The rest of the elements of $\boldsymbol{U}$ are zero. Then, for example, if we want to recover the i ascending branch, we need to plot $(\boldsymbol{H}[k,i], \boldsymbol{U}[k,i])$ for $k = i$ to $n - 1$.

3.1.4. The NFP data treatment

The goal of the preprocessing effort is to build a new matrix $\boldsymbol{N}$, with the information of the AB and DB of the NFP, identical to $\boldsymbol{U}$. For this purpose, we need to use four auxiliary matrices, two associated to the ascending branches: $\boldsymbol{NA}$ and $\boldsymbol{HA}$, and two to the

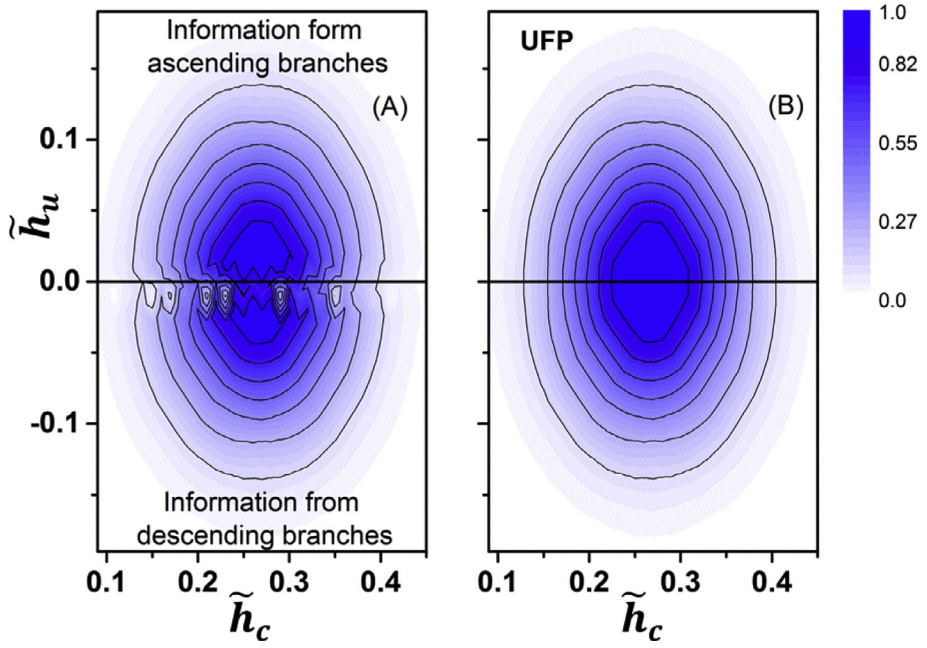

Fig. 4. FORC diagrams built from data of Fig. 3. Left panel: FORC diagram as a result of the union of the ascending and descending branches information. Right panel: traditional diagram of the UFP. The $h_u \sim 0$ region of the panel (A) shows loss of information.

descending branches: ***ND*** and ***HD***. These are matrices of $n \times n1$ range, where $n1 = (n + nmod(2))/2$. The expression $p \ mod(n) = q$ indicates the rest of the quotient $p/n = q$ which p,n and q integers. The rules for the construction of the above mentioned matrices follow the same "spirit" of the ***H*** and ***U*** ones, with the corresponding changes due to the differences in the experimental data recording between both protocols. The ***NA*** and ***HA*** are constructed according the following expressions:

$$\begin{cases} \boldsymbol{HA}[\boldsymbol{i},\boldsymbol{j}] = \begin{cases} H_{min} + i\Delta & if \quad (n-j) > i \geqslant j \\ 0 & otherwise \end{cases} \\ \boldsymbol{NA}[\boldsymbol{i},\boldsymbol{j}] = \begin{cases} M_j(H_{min} + i\Delta) & if \quad (n-j) > i \geqslant j \\ 0 & otherwise \end{cases} \end{cases} \tag{5}$$

where j goes from 0 to $n1 - 1$. $M_j(H)$ represents the magnetization of the j ascending branch at the H field.

On other hand, the ***ND*** and ***HD*** matrices are built according to the following rules:

$$\begin{cases} \boldsymbol{HD}[i,j] = \begin{cases} H_{min} + i\Delta & if \quad (n-j) \geqslant i \geqslant j > 0 \\ 0 & otherwise \end{cases} \\ \boldsymbol{ND}[i,j] = \begin{cases} M_j(H_{min} + i\Delta) & if \quad (n-j) \geqslant i \geqslant j > 0 \\ 0 & otherwise \end{cases} \end{cases} \tag{6}$$

where j goes from 1 to $n1 - 1$. Note that, at variance with the ascending case, the first descending branch is labeled as 1 ($M_j(0)$ does not exist).

As in the case of the ***H*** and ***U*** matrices, $(\boldsymbol{HA}[k,i], \boldsymbol{NA}[k,i])$ and $(\boldsymbol{HD}[k,i], \boldsymbol{ND}[k,i])$ have the information about the i ascending and descending branches, respectively, with the particularity that the descending branches are presented in a sense opposite to the real measurement. To illustrate the matrix construction, we show a scheme of ***HA***, ***NA***, ***HD*** and ***ND*** matrices in Fig. 5. In these matrices

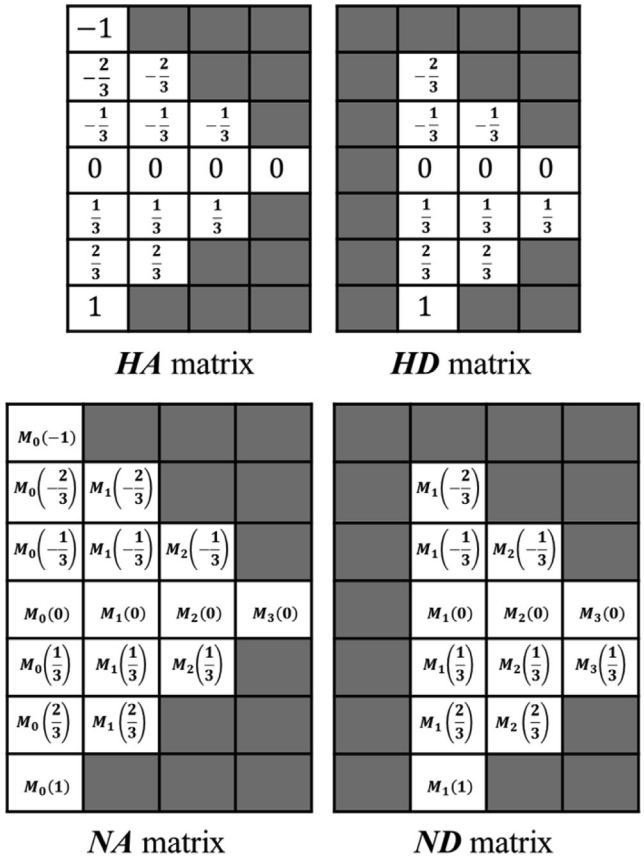

Fig. 5. Schematic representation of the ascending (***HA*** and ***NA***) and descending (***HD*** and ***ND***) matrices for the case $n = 7$ corresponding to Fig. 2.

the value $M_i(h)$ represents the magnetization of the branch i at the h field. In all cases shaded boxes indicate null elements that will not be taken into account in the data processing protocol. We can observe that, at variance with the ***H*** and ***U*** matrices, the new

ones do not present a triangular inferior shape. To simplify the notation of the algorithm we have labeled as "1" the first DB and as "0" the first AB. As in the case of Fig. 3, the magnetic field is normalized by its maximum value and we are assuming (which it is not strictly necessary, but it is usual in the FORC procedure) that $H_{min} = -H_{max}$. Although n is an odd number in the example, it could also be even.

The first step in order to build the ***N*** matrix is to use the information of the ***NA*** matrix. For this it is necessary to introduce some definitions, which will be used in the description of the algorithm:

We define the ascending difference vector $D_k[i]$, of $nD = dim(D_k) = n - 2k$ elements built according to the rule:

$$D_k[i] = \begin{cases} \boldsymbol{NA}[i,0] & if\ k = 0 \\ \boldsymbol{NA}[i,k] - \boldsymbol{NA}[i,k-1] & if\ k > 0 \end{cases} \tag{7}$$

with $i = k, \ldots, n-(k+1)$; and $k = 0, \ldots, n1-1$. The k value indicates at which column of ***NA*** (and also ***N***) the $D_k[i]$ vector is associated.

We will call propagate the $D_k[i]$ vector into the ***N*** matrix to the following procedure:

$$\begin{aligned} &\text{for} j = k, \ldots, n-(1+k) \text{do} \\ &\{ \\ &\quad \text{for} i = j, \ldots, n-(k+1) \text{do} \\ &\quad \{ \\ &\qquad \boldsymbol{N}[i,j] = \boldsymbol{N}[i,j] + D_k[i] \\ &\quad \} \\ &\} \end{aligned} \tag{8}$$

As shown in expression (8) it is important to sweep i and j in the correct order.

With the above definitions in mind, we will proceed as follow:

(1) Set all the elements of ***N*** to zero. $\boldsymbol{N}[i,j] = 0$ for $i = 0, \ldots, n-1$ and $j = 0, \ldots, n-1$.
(2) For $k = 0$ to $n1-1$:
  (A) Create the $D_k[i]$ vector according to Eq. (7).
  (B) Propagate the $D_k[i]$ vector into the ***N*** matrix following the procedure given by expression (8).

Note that in the case $k = 0$, the propagation of $D_0[i]$ into the ***N*** matrix results in the fact that the first column of the ***N*** matrix becomes equal to the first of the ***NA*** matrix.

To complete the ***N*** matrix we need to use the ***ND*** information (corresponding to the descending branch of the NFP). In the case of the ascending branch processing, using the matrix ***NA***, the idea was to propagate the information from the lower ascending branches towards the upper ones. In the same way, for the descending branches the spirit of the algorithm is to propagate the information from the higher descending branches towards the lower ones using the matrix ***ND***.

There are two important differences between the matrices ***HA*** and ***HD*** which makes it necessary to modify the structure of the above mentioned algorithm for the case of the DB treatment. The first one is the fact that the first column of the ***HA*** matrix exactly matches with the corresponding to the ***H*** matrix, contrary to what happens with the ***HD*** one (see Fig. 5). The second difference is that despite in both ***HA*** and ***HD*** matrices the field of a given column (branch) increases as we advance in the column, the branches of ***HD*** are measured in the opposite direction. For these reasons we are forced to modify the previous algorithm and definitions in order to adapt them to the treatment of the information contained in the ***HD*** and ***ND*** matrices. We then these reasons introduce the following concepts:

- We will use a descending difference vector $d_k[i]$ of $nd = dim(d_k) = n + 1 - 2k$ elements, given by:

$$d_k[i] = \boldsymbol{ND}[i,k-1] - \boldsymbol{ND}[i,k] \tag{9}$$

  with $i = k, \ldots, n-k$, and $k = 2, \ldots, n1-1$. As in the case of the ascending difference vector, the k index indicates the associated column.
- From each $d_k[i]$ vector we obtain nd new vectors $\delta_{k,\beta}[j]$, with $\beta = k, \ldots, n-k$, and dimension $n\delta = dim(\delta_{k,\beta}) = n + 1 - (k+\beta)$, spanning from nd $(\beta = k)$ to 1 $(\beta = n-k)$. Each one of these $\delta_{k,\beta}[j]$ vectors has all of their elements equal, and given by the following expression:

$$\delta_{k,\beta}[j] = \begin{cases} d_k[\beta] & \beta = k \\ d_k[\beta] - d_k[\beta-1] & \beta > k \end{cases} \tag{10}$$

  for $j = \beta, \ldots, n-k$.
- As in the case of the vector D_k, we call propagate the vector $\delta_{k,\beta}$ into the ***N*** matrix to the following procedure:

$$\begin{aligned} &\text{for} \beta = k, \ldots, n-k \text{do} \\ &\{ \\ &\quad \text{for} i = \beta, \ldots, n-k \text{do} \\ &\quad \{ \\ &\qquad \boldsymbol{N}[i,\beta] = \boldsymbol{N}[i,\beta] + \delta_{k\beta}[i] \\ &\quad \} \\ &\} \end{aligned} \tag{11}$$

With these concepts and definitions in mind, we can describe the second part of the pre-processing protocol:

(1) For $k = 2$ to $n1-1$:
  (A) Create the $d_k[i]$ vector according to Eq. (9). For each of their nd components:
    (A1) Create the $\delta_{k,\beta}[j]$ vector according to the instructions of Eq. (10).
    (A2) Propagate the vector $\delta_{k,\beta}$ into the ***N*** matrix.

Then, following these steps we can build the ***N*** matrix, which should be identical to ***U***, using the ***NA*** and ***ND*** matrices information.

The ideas behind of the algorithm, as well as a detail discussion about the no loss of information in the NFP respect the UFP are given in the Appendix I: Grounds of the algorithm.

4. Numerical results

With the same data of the example corresponding to Figs. 3 and 4, we show in Fig. 6 the result of a FORC diagram using the NFP. Panel (A) shows the AB built in the construction of the ***N*** matrix. They are identical to those corresponding to the UFP (see Fig. 3 (A)). Dashes lines (horizontal and vertical) in panel (B) indicate the cross sections performed to obtain h_c and H_{int} distributions. The horizontal cross corresponds to the h_C distribution, and the vertical one to H_{int}. In all cases the distributions have been normalized by their maximum value to 1. We can observe that the results are exactly the same for both methods, the UFP and NFP. This was also confirmed numerically by the fact that the ***U*** and ***N*** matrices are identical. This fact is also reflected in the h_C and H_{int} distributions obtained by these methods, which correspond almost exactly with the input information.

We want to present another numerical example in which both protocols were used. The calculations were performed for both methods, the traditional one (UFP) and for the new one. The results

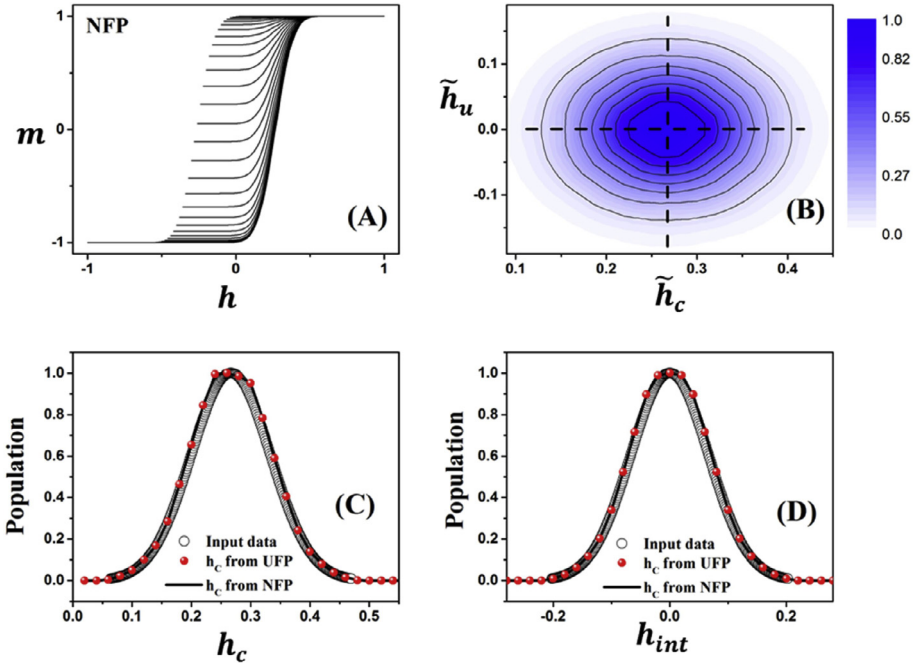

Fig. 6. Results of the new FORC processing for the example of Fig. 3. Panel (A) shows the ascending branches built form the AB and DB of the NFP. Panel (B): FORC diagram. Panel (C): Comparison of the h_c distribution input data with the one obtained from the UFP and NFP. Panel (D): Comparison of the H_{int} distribution input data with that one obtained from the UFP and NFP.

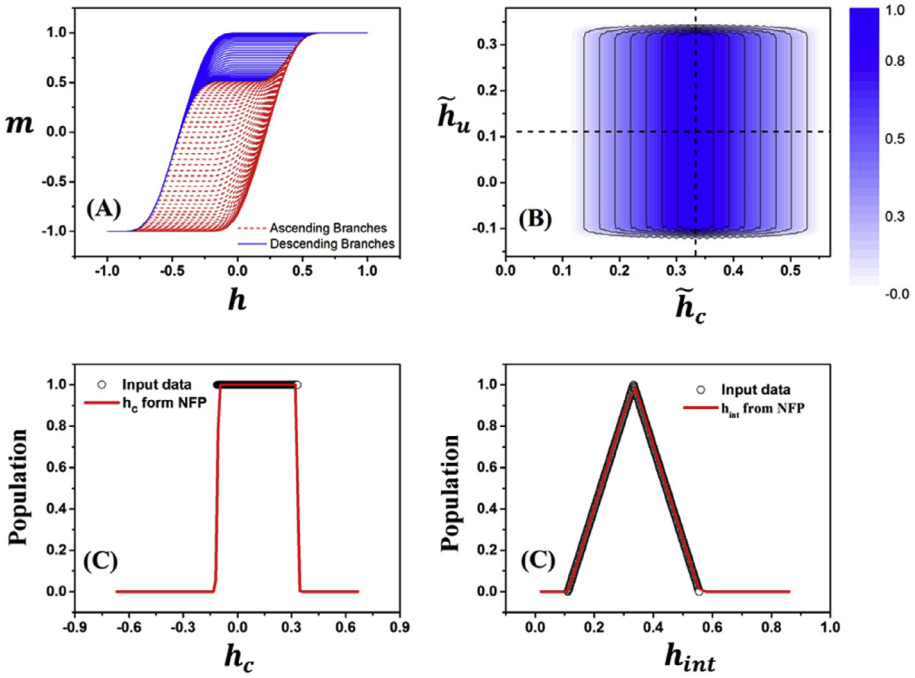

Fig. 7. Numerical example of the use of NFP. The input h_c and H_{int} distributions are non-soft functions. Panel (A): ascending and descending branches. Panel (B): FORC diagrams. Panel (C): Comparison of the h_c distribution input data with the one obtained from the NFP. Panel (D): Comparison of the H_{int} distribution input data whit the obtained from the NFP.

were numerically indistinguishable, whereby, only those corresponding to the NFP are shown. In this case, with the idea of test the proposed protocol, we used two unusual distributions for h_c and H_{int}. The first one is uniform, while the second one has a triangular profile. The results of the simulations are illustrated in Fig. 7. Panel (A) shows the AB and DB, panel (B) shows the FORC diagram, and panels (C) and (D) the results of the h_c and H_{int} distributions compared with the input data. The dashed lines (horizontal and vertical) in panel (B) indicate the cross sections performed for obtain the h_c and H_{int} distributions. In this case, at variance with Fig. 4, the irreversibility mean field distribution is displaced from zero. For this reason the occupied area of the AB is greater than the DB in panel (A). From the rest of the panel we can observe that the numerical results do not exhibit anomalies, and also the distri-

butions obtained from the FORC diagram of panel (B) are very close to the input data, even in the case of these anomalous distributions.

Other numerical examples with different kinds of h_c and H_{int} distributions (lognormal, normal, etc.) has been used for build their FORC diagrams using both methods. In all cases the numerical results has been exactly the same, without difference between both FORC constructions.

5. NFP and UFP in real systems

We have discussed the use of the NFP and compared it with the UFP within the hypothesis of the five postulates given in the Section 3. We want to mention some features that we could expect when applying both method to real systems, or in magnetic systems that do not satisfy the above mentioned postulates. The first observation is that both methods could not give equal results. For example, it is known that for the case in which the easy axes are not along the orientation of the magnetic field, the UFP diagram shows some anomalous and spurious information[26] due to a particular curvature in the hysteresis loops of each magnetic entity. We observed these artifacts, with some differences, in numerical simulation using the NFP (not shown in this work). Another important case occurs when the interactions are state dependent, that is, the interaction between two magnetic entities depends on the magnetic state of both. In this case we also expect to find differences between the FORC diagrams of the UFP and NFP. These differences appear as a consequence of the different paths that each method has to reach a given magnetic point. One could ask which method gives a better description of the magnetic characteristics. The answer is that a priori it is not possible to elucidate this, because the interpretation that the system can be characterized by their coercive and interactions field distributions is based on the hypothesis of state independent interaction. For more clarity, consider the case of the UFP. In this case, the magnetization of one particular hysteron, as a function of H and H_0 (see Section 3) can be expressed as:

$$m(H_0,H,H_c,H_{int}) = 2\theta(H_0+H_{int}+H_c)[1-\theta(H+H_{int}-H_c)] + 2\theta(H+H_{int}-H_c)-1 \quad (12)$$

where $\theta(x)$ is the Heaviside step function.

Observe that in this expression, the interaction field H_{int} is the same when the system is under H_0 and H fields, according to the second postulate of Section 3. Then, using the m expression in Eq. (2), the calculated FORC distribution according to Eq. (1) definition, and using the $\tilde{H}_c$ and $\tilde{H}_u$ definition we obtain:

$$\rho(\tilde{H}_c,\tilde{H}_u) = \left\{\sum_j f(H_c^j)\delta(\tilde{H}_c-H_c^j)\right\}\left\{\sum_k g(H_{int}^k)\delta(\tilde{H}_u-H_{int}^k)\right\} \quad (13)$$

This result shows that the information about $f(H_c^j)$ and $g(H_{int}^k)$ is contained in the $\tilde{H}_c$ and $\tilde{H}_u$ axis respectively. However, if H_{int}^k depends on the state of the system, the expression (13) is modified, and the deltas become:

$$\begin{cases} \delta(\tilde{H}_c-H_c^j) \to \delta(\tilde{H}_c-H_c^j+(H_{int}^k(H_0)-H_{int}^k(H))/2) \\ \delta(\tilde{H}_u-H_{int}^k) \to \delta(\tilde{H}_u-(H_{int}^k(H_0)+H_{int}^k(H))/2) \end{cases} \quad (14)$$

Then, the factorization of Eq. (13) is lost. The same problems appear in the NFP, which prevents to choose, a priori, one method over the other. The differences can be greater if, for example, the coercitive field also depends on the interactions. In effect, in real system the FORC diagrams cannot understand as the description of a collection of non-interacting hysterons. These diagrams become a "fingerprint" of the magnetic characteristics of the system. In this sense, the new method could offer a different "fingerprint". This fact opens a new possibility for a deeper study of the characteristic interactions and also their effects on the coercitive field.

6. Conclusions

In this work we have presented a modified protocol to generate FORC diagrams. The protocol consists in an adapted measurement recipe and an algorithm for data pre-processing. We have shown that the new method and the usual one give exactly the same information if the system under study is described by the Stoner-Wohlfarth model with an interaction field distribution as in the Preisach-type models. Numerical simulations have confirmed this fact, even in the case of anomalous or non-conventional field distributions.

The use of the new method implies an important experimental time saving. It requires an small additional effort of data pre-processing, after which, the data treatment is identical to the usual method.

We have also considered in our discussion the case in which the interactions are state-dependent and conclude that it is possible to find a difference between the traditional method and the proposed one. Even though this fact prevents the choice of the appropriated method, it opens interesting possibilities for future studies in order to gain a deep understanding on the interaction and coercive fields description of magnetic materials.

Acknowledgements

The author acknowledges from CONICET Argentina, SECyTP – Universidad Nacional de Cuyo (C006 and 06/C464), and PICT –2012-00492 (Foncyt) subsides. The author wants to thanks professors Alejandro Butera and Carlos Ramos by the careful reading of the manuscript.

Appendix I.

A.I. Grounds of the algorithm

After giving the algorithm to process the data of the ascending and descending branches, we will explain the idea that motivates it. Some concepts were already exposes, but now we will give a constructive explanation of the algorithm summarized in Eqs. (7)–(11). In addition, we will also discuss the non-loss of information associated to the pre-processing carried out in the case of the NFP. In order to perform this analysis, we will introduce an appropriate nomenclature to refer to the ascending and/or descending branches, as well as to the initial and final fields. Unless otherwise indicate we will refer to branches as those associated to the NFP. We will referred to the ascending branch k as R_k, and the descending one as r_k. The initial and final fields of R_k will be refer as HR_i^k and HR_f^k respectively. Consistently with this, the initial and final fields of r_k are mentioned as hr_i^k and hr_f^k respectively. In addition, following this convention of uppercase and lowercase letters, $M_k(h)$ and $m_k(h)$ indicate the value of the magnetization at the h field corresponding to the k ascending and descending branches respectively.

We will start the analysis from the AB of the ***NA*** matrix. Due to the fact that the first ascending branch is the same for UFP and NFP, this will be the first brick of our construction and is placed as the first column of the matrix ***N***. The first column is then propagated towards the rest of the matrix according to the procedure given in Eq. (8). This implies that all branches of ***N*** are equal to R_1, except,

of course, for the initial field of each branch. Let us now imagine the case where all ascending branches $(R_2, R_3, \ldots, R_{n-1})$ of the ***NA*** matrix were measured up to $h_{max} = 1$, as it happens in the UFP. In this hypothetical case, computing the difference between R_2 and R_1 branches generates the $D_2[i]$ vector (i runs over the rows), which is added to the second column of ***N*** ($\boldsymbol{N}[i,2] = \boldsymbol{N}[i,2] + D_2[i]$) we will obtain in the second column of ***N*** all the information of the second ascending branch corresponding to the UFP. We continue until we propagate this information over the rest of the ***N*** matrix. By repeating this procedure for each of the ascending branches we would have in the ***N*** matrix all the required information. This is the "spirit" of the pre-processing ascending algorithm, to propagate the information of the ascending branches successively on the ***N*** matrix.

However, in the new protocol, the final field of the ascending k branch, H_f^k does not achieve the H_{max} value, but reduced as we advance in k, the branch number. In other words, we are "losing" the last rows of ***NA*** as we increase k. We want to show that, under the hypothesis of the proposed model, the above mentioned fact does not imply loosing information for the successive branches. Let $h^* > 0$ be the irreversibility field, defined as the field above which the magnetic system has not longer an irreversible response, i.e., the magnetization of the branches collapse in a unique curve for $h > h^*$. While we work in branches that satisfy $RH_f^j \geqslant h^*$, it's obvious that the successive decrease of the final field value RH_f^j, does not imply a loss of information. In these cases, for fields $h > RH_f^j$ (which are not accessible for the NFP) we have that[27] $D_j[i] = 0$ for $i > j$. In other words, the difference between the branches for $h > RH_f^j$ is null, because there is not hysteresis. Then, the above mentioned procedure to propagate a given column to the rest of the matrix is enough to retrieve the information which is not contained in a given branch, but in its predecessors. Now suppose the case in which the R_k and R_{k+1} branches satisfies $RH_f^k \geqslant h^*$ and $RH_f^{k+1} < h^*$. In this case we don't have problems, because $D_{k+1}[i] = 0$ for $h > RH_f^{k+1}$, due to the fact that the field next to RH_f^{k+1} is RH_f^k. For the next branches we should remember that, according to our assumption, the magnetization at $h = RH_f^{k+1}$ is irreversible, then $m_k(h) > M_{k+1}(h)$, which means that variation of magnetization $\Omega = m_k(h) - M_{k+1}(h)$ is positive, as illustrated[28] in Fig. 8. The difference Ω comes from the contribution of a group of hysterons that reverse their magnetization from up to down at HR_i^k (that is at the beginning of the R_k), but they do not reverse at the beginning of R_{k+1}. All the ascending branches R_t that follow the R_k (with $t > k$) satisfy $HR_i^t > HR_i^k$, and the before mentioned hysterons remain up in the rest of the protocol development (based on the second and third hypotheses of the model). For this reason, their contribution to the magnetization will be constant (and was already taken into account when we computed the $D_{k+1}[i]$ differences). Then, we can ignore their contribution to the hysteresis. This fact allows us to imagine a new situation in which, for practical purposes, the irreversibility field is $h^* = HR_i^{k+1}$. Then, we can apply the previous reasoning to the new situation, which means that there is no loss of information. Obviously, this reasoning can be performed for each of the ascending branches R_t with $t > k + 1$. This argument demonstrates our assertion that there is no loss of information by the successive decrease of the field sweep in each branch.

In reference to the processing of the descending branches, we can assert that the reasoning is very similar to that of ascending branches exposed before. The idea is to complete the information of the ***N*** matrix, based in the difference between the descending branches,. However, there are two important differences with respect to the case of the ascending branches. The first one is that when we are moving forward in the descending branch number, the magnetization decreases. This is reflected on the definition of $d_k[i]$ in Eq. (9), because the computed difference is from the previous branch minus the next branch, unlike in the Eq. (7), which gives the definition of $D_k[i]$. The second difference is the fact that the field is diminishing as we advance in each descending branch. This fact modifies the processing with respect to the case of the ascending branches. For convenience we choose to generate the ***HD*** and ***ND*** matrices in a similar fashion to ***HA*** y ***NA***, that is: when we advance along a given column of ***HD***, the field is increased. This results in the need to modify the recipe for the propagation of a given column, as is given in Eqs. (9)–(11) for the case of the descending branches. The opposite sense in the field sweeping in the descending branches makes necessary to define $\delta_{k,\beta}[j]$ from $d_k[i]$ in order to propagate the information.

Finally, the argument used in the discussion of the no loss of information in the case of the ascending branches is also valid in this case, due to the symmetry of the problem.

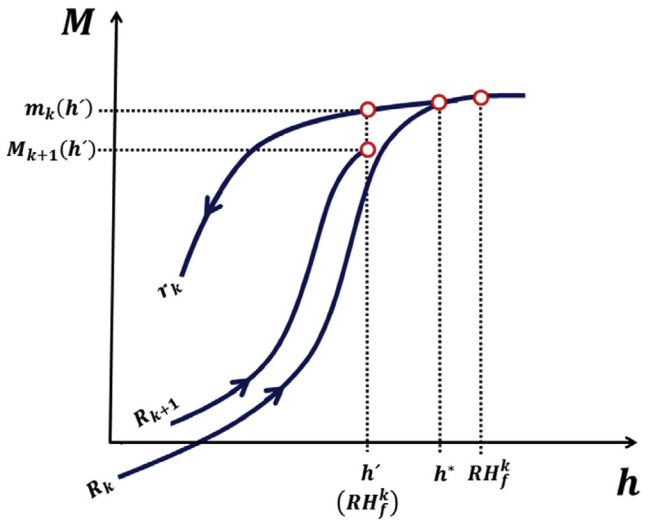

Fig. 8. Schematic representation of ascending and descending branches in the field irreversibility region of the hysteresis loop. Due to the characteristics of the new measurement protocol, the irreversibility does not imply information loss (see text on the Appendix I).

References

[1] A.R. Muxworthy, A.P. Roberts, Encyclopedia of Geomagnetism and Paleomagnetism, Springer, Netherlands, 2007.

[2] C.-I. Dobrotă, A. Stancu, Tracking the individual magnetic wires' switchings in ferromagnetic nanowire arrays using the first-order reversal curves (FORC) diagram method, Phys. B Condens. Matter. 457 (2015) 280.

[3] S. Samanifar, M. Almasi Kashi, A. Ramazani, M. Alikhani, Reversal modes in FeCoNi nanowire arrays: correlation between magnetostatic interactions and nanowires length, J. Magn. Magn. Mater. 378 (2015) 73.

[4] M. Almasi-Kashi, A. Ramazani, M. Amiri-Dooreh, FORC investigation of as-deposited and annealed CoZn alloy nanowires, Phys. B Condens. Matter. 452 (2014) 124.

[5] D.A. Gilbert et al., Quantitative decoding of interactions in tunable nanomagnet arrays using first order reversal curves, Sci. Rep. 4 (2014) 1.

[6] M. Pan, P. Zhang, H. Ge, N. Yu, Q. Wu, First-order-reversal-curve analysis of exchange-coupled SmCo/NdFeB nanocomposite alloys, J. Magn. Magn. Mater. 361 (2014) 219.

[7] D. Cimpoesu, I. Dumitru, A. Stancu, Kinetic effects observed in dynamic first-order reversal curves of magnetic wires: experiment and theoretical description, J. Appl. Phys. 120 (2016) 173902.

[8] M. Pohlit et al., First order reversal curves (FORC) analysis of individual magnetic nanostructures using micro-hall magnetometry, Rev. Sci. Instrum. 87 (2016) 113907.

[9] X.T. Zhao et al., Weak dipolar interaction between CoPd multilayer nanodots for bit-patterned media application, Mater. Lett. 182 (2016) 185.

[10] N.S. Bezaeva et al., The effects of 10 to 160 GPa shock on the magnetic properties of basalt and diabase, Geochem. Geophys. Geosyst. 17 (2016) 4753.

[11] A.H. Montazer et al., Developing high coercivity in large diameter cobalt nanowire arrays, J. Phys. D. Appl. Phys. 49 (2016) 445001.
[12] M. Alikhani, A. Ramazani, M. Almasi Kashi, S. Samanifar, A.H. Montazer, Irreversible evolution of angular-dependent coercivity in Fe80Ni20 nanowire arrays: Detection of a single vortex state, J. Magn. Magn. Mater. 414 (2016) 158.
[13] S. Kobayashi et al., Investigation of effects of long-term thermal aging on magnetization process in low-alloy pressure vessel steels using first-order-reversal-curves, AIP Adv. 7 (2017) 56002.
[14] L. Yu et al., Magnetization Reversal of Three-Dimensional Nickel Anti-Sphere Arrays, IEEE Magn. Lett. 8 (2017) 1.
[15] Q. Li et al., Rock magnetic properties of the Lz908 borehole sediments from the southern Bohai Sea, eastern China, Chin. J. Geophys. (Acta Geophys. Sin.) 59 (2016) 1717.
[16] A.P. Roberts, C.R. Pike, K.L. Verosub, First-order reversal curve diagrams: a new tool for characterizing the magnetic properties of natural samples, J. Geophys. Res. Solid Earth 105 (2000) 28461.
[17] C. Kissel, Z. Liu, J. Li, C. Wandres, Magnetic minerals in three Asian rivers draining into the South China Sea: Pearl, Red, and Mekong Rivers, Geochem. Geophys. Geosyst. 17 (2016) 1678.
[18] E. De Biasi, J. Curiale, R.D. Zysler, Quantitative study of FORC diagrams in thermally corrected Stoner– Wohlfarth nanoparticles systems, J. Magn. Magn. Mater. 419 (2016) 580.
[19] M.P. Proenca et al., Identifying weakly-interacting single domain states in Ni nanowire arrays by FORC, J. Alloys Compd. 699 (2017) 421.
[20] F. Béron et al., Nanometer scale hard/soft bilayer magnetic antidots, Nanoscale Res. Lett. 11 (2016) 1.
[21] X. Zhao, D. Heslop, A.P. Roberts, A protocol for variable-resolution first-order reversal curve measurements, Geochem. Geophys. Geosyst. 1364 (2015).
[22] C.R. Pike, A.P. Roberts, K.L. Verosub, C.R. Pike, A.P. Roberts, Characterizing interactions in fine magnetic particle systems using first order reversal curves Characterizing interactions in fine magnetic particle systems using first order reversal curves, J. Appl. Res. 85 (1999) 6660.
[23] Note that the last point of the chain is also represented by an open square dot, because it represents the last link of the descending branch and the initial link of the last chain.
[24] I.D. Mayergoyz, Mathematical Models of Hysteresis, Springer, New York, 1991, pp. 1–63.
[25] E. Della Torre, Magnetic Hysteresis, IEEE Press, 1999.
[26] A.J. Newell, A high-precision model of first-order reversal curve (FORC) functions for single-domain ferromagnets with uniaxial anisotropy, Geochem. Geophys. Geosyst. 6 (2005) Q05010.
[27] Note that the $D_j[i]$ vector does not have components for $i > j$, according to their definition in equation 7. The paragraph indicates that if we extend the range of the vector, their components that satisfy $i > j$ will be null, because the magnetic branches have the same magnetization values for the same fields $h > RH_f^j$.
[28] Note that it may happen that $M_{k+1}(h') > M_k(h')$ or $M_{k+1}(h') = M_k(h)$, but what will always happen is that, according to the definition of $h^* \ \Delta > 0$, that is $m_k(h') > M_{k+1}(h')$.